Accepted Manuscript

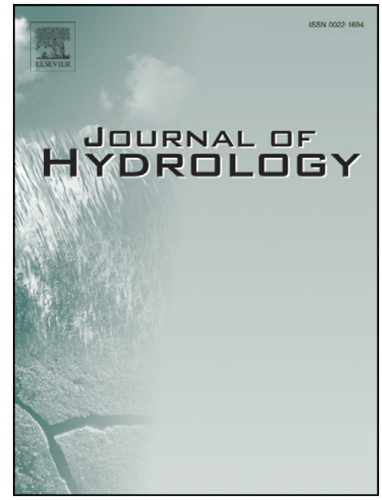

Modeling the effect of clay drapes on pumping test response in a cross-bedded aquifer using multiple-point geostatistics

Marijke Huysmans, Alain Dassargues

PII: S0022-1694(12)00380-0
DOI: http://dx.doi.org/10.1016/j.jhydrol.2012.05.014
Reference: HYDROL 18232

To appear in: *Journal of Hydrology*

Received Date: 2 March 2012
Revised Date: 2 May 2012
Accepted Date: 7 May 2012

Modeling the effect of clay drapes on pumping test response in a cross-bedded aquifer using multiple-point geostatistics

Marijke Huysmans[(1)] (corresponding author) and Alain Dassargues[(1,2)]

[(1)] Katholieke Universiteit Leuven
Applied Geology and Mineralogy
Department of Earth and Environmental Sciences
Celestijnenlaan 200 E
3001 Heverlee
Belgium
Tel: +32 16 32 64 49
Fax: +32 16 32 29 80
E-mail: marijke.huysmans@ees.kuleuven.be

[(2)] Université de Liège
Hydrogeology and Environmental Geology
Department of Architecture, Geology, Environment, and Civil Engineering (ArGEnCo)
B.52/3 Sart-Tilman
4000 Liège
Belgium

Abstract

This study investigates whether fine-scale clay drapes can cause an anisotropic pumping test response at a much larger scale. A pumping test was performed in a sandbar deposit consisting of cross-bedded units composed of materials with different grain sizes and hydraulic conductivities. The measured drawdown values in the different observation wells reveal an anisotropic or elliptically-shaped pumping cone. The major axis of the pumping ellipse is parallel with the strike of cm to m-scale clay drapes that are observed in several outcrops. To determine (1) whether this large-scale anisotropy can be the result of fine-scale clay drapes and (2) whether application of multiple-point geostatistics can improve interpretation of pumping tests, this pumping test is analysed with a local 3D groundwater model in which fine-scale sedimentary heterogeneity is modelled using multiple-point geostatistics. To reduce CPU and RAM demand of the multiple-point geostatistical simulation step, edge properties indicating the presence of irregularly-shaped surfaces are directly simulated. Results show that the anisotropic pumping cone can be attributed to the presence of the clay drapes. Incorporating fine-scale clay drapes results in a better fit between observed and calculated drawdowns. These results thus show that fine-scale clay drapes can cause an anisotropic pumping test response at a much larger scale and that the combined approach of multiple-point geostatistics and cell edge properties is an efficient method for integrating fine-scale features in larger scale models.

Keywords: Multiple-point geostatistics; Groundwater Flow; Heterogeneity; Pumping test; Upscaling; Cross-bedding

Highlight 1: Fine-scale clay drapes can cause anisotropic pumping test response at larger scale

Highlight 2: An approach using multiple-point geostatistics and edge properties is proposed

Highlight 3: Incorporating fine-scale clay drapes results in a better fit of drawdowns

1. Introduction

Clay drapes are thin irregularly-shaped layers of low-permeability material that are often observed in different types of sedimentary deposits (Reineck and Singh 1973). Their thicknesses are often only a few centimetres (Houthuys 1990; Stright 2006). Despite their limited thicknesses, several studies indicate that they may influence subsurface fluid flow and solute transport at different scales (Ringrose et al. 1993; Willis and White 2000; Morton et al. 2002; Mikes 2006; Stright 2006; Li and Caers 2011; Huysmans and Dassargues 2009). It seems that structural heterogeneity (such as clay drapes) at fine scale might yield anisotropy at large scale, whereas “random" heterogeneity may yield an isotropic behavior at large scale. However, many studies show that the effect of fine-scale heterogeneity is limited to fine scales and averaged out on larger scales and that consequently the type of geological heterogeneity that needs to be taken into account depends on the scale of the problem under consideration (Schulze-Makuch and Cherkauer 1998; Schulze-Makuch et al. 1999; Beliveau 2002; Neuman 2003; Eaton 2006). Van den Berg (2003) found for example that anisotropy caused by lamination is small compared to the influence of larger scale heterogeneities so that these sedimentary structures only cause anisotropy on a smaller scale. It is therefore unclear whether centimeter-scale clay drapes can influence groundwater flow and solute transport at scales exceeding the meter-scale. This study therefore investigates whether fine-scale clay drapes can cause an anisotropic pumping test response at a much larger scale. This study is based on measured drawdown values from a pumping that reveal an anisotropic or elliptical-shaped pumping cone: the major axis of the pumping ellipse is parallel with the strike of the centimetre to meter-scale clay drapes that are observed and measured in several outcrops and quarries. This study quantitatively investigates whether this large-scale anisotropy can be the result of fine-scale clay drapes.

It is very difficult to incorporate clay drapes in aquifer or reservoir flow models, because of their small size and the complexity of their shape and distribution. In standard upscaling approaches (Renard and de Marsily 1997; Farmer 2002), the continuity of the clay drapes is not preserved (Stright 2006). Multiple-point geostatistics is a technique that has proven to be very suitable for simulating the spatial distribution of such complex structures (Strebelle 2000; Strebelle 2002; Caers and Zhang 2004; Hu and Chugunova 2008; Huysmans and Dassargues, 2009; Comunian et al. 2011; dell'Arciprete et al. 2012). Multiple-point geostatistics was developed for modelling subsurface heterogeneity as an alternative to variogram-based stochastic approaches that are generally not well suited to simulate complex, curvilinear, continuous, or interconnected structures (Koltermann and Gorelick 1996; Fogg et al. 1998; Journel and Zhang 2006). Multiple-point geostatistics overcomes the limitations of variogram by directly inferring the necessary multivariate distributions from training images (Guardiano and Srivastava 1993; Strebelle and Journel 2001; Strebelle 2000; Strebelle 2002; Caers and Zhang 2004; Hu and Chugunova 2008). In this way, multiple-point geostatistics provides a simple mean to integrate a conceptual geological model in a stochastic simulation framework (Comunian et al., 2011). In the field of groundwater hydrology, application of multiple-point geostatistics to modeling of groundwater flow and transport in heterogeneous media has become an active research topic in recent years. Feyen and Caers (2006) apply the method to a synthetic two-dimensional case to conclude that the method could potentially be a powerful tool to improve groundwater flow and transport predictions. Several recent studies apply the method to build realistic (hydro)geological models based on field observations on geological outcrops and logs (Huysmans et al. 2008; Ronayne et al. 2008; Huysmans and Dassargues 2009; Bayer et al. 2011; Comunian et al. 2011; Le Coz et al. 2011; dell'Arciprete et al. 2012). In large-scale three-dimensional grids multiple-point geostatistics may be computationally very intensive. Several studies focus on improved implementations of the multiple-point statistics techniques to make the algorithms more powerful and computationally efficient (e.g., Mariethoz et al. 2010; Straubhaar et al. 2011). Huysmans and Dassargues (2011) developed the method of "direct multiple-point geostatistical simulation of edge properties" which enables simulating thin irregularly-shaped surfaces with a smaller CPU and RAM demand than the conventional multiple-point statistical methods. This method has been applied on simple test cases (Huysmans and Dassargues 2011) and the present study is the first to apply the method of "direct multiple-point geostatistical simulation of edge properties" to a full-scale three-dimensional groundwater model. In this way, this study investigates whether the combined approach of using multiple-point geostatistics and edge properties is an efficient and valid method for integrating fine-scale features in larger scale models.

A last scientific goal of this paper is to determine the added benefits of explicitly incorporating clay drape presence for inverse modelling of pumping tests. Several authors have shown that incorporating heterogeneity can result in improved correspondence between calculated and observed hydraulic heads (e.g., Herweijer 1996; Lavenue and de Marsily 2001; Kollet and Zlotnik 2005; Ronayne et al. 2008; Harp and Vesselinov 2011). However, some authors show that incorporating additional data about heterogeneity does not always result in better calibration (e.g., Hendricks Franssen and Stauffer 2005). This paper quantifies the change in calibration error when clay drapes are incorporated in groundwater flow models.

2. Material and methods

The methodology followed in this study consists of the following steps. First, field data are obtained in an extensive field campaign mapping sedimentary heterogeneity and fine-scale air permeability. Secondly, a training image displaying clay drape occurence is constructed based on the geological and hydrogeological field data obtained from this field campaign. Thirdly, this training image with small pixel size is converted into an upscaled edge training image which is used as input training image to perform multiple-point SNESIM (Single Normal Equation SIMulation) simulations. The SNESIM algorithm (Strebelle 2002) allows borrowing multiple-point statistics from the training image to simulate multiple realizations of facies occurrence. SNESIM is a pixel-based sequential simulation algorithm that obtains multiple-point statistics from the training image, exports it to the geostatistical numerical model, and anchors it to the actual subsurface hard and soft data. In this study, the resulting simulations indicate at which cell edges horizontal or vertical clay drapes are present. This information is incorporated in a local 3D groundwater model of the pumping test site by locally adapting vertical leakance values and by locally inserting horizontal flow barriers. All hydraulic parameters including the clay drapes properties are calibrated using the measured drawdown time series in six observation wells.

2.1 Geological setting

The pumping test site is situated in Bierbeek near Leuven (Belgium) as shown in Figure 1. The subsurface geology in this area consists of a 4m-thick cover of sandy loam from Pleistocene age, 35m of Middle-Eocene Brussels Sands and 12 m of low permeable Early-Eocene Ieper Clay (Figure 2). At the pumping test site the Brussels Sands aquifer acts as an unconfined aquifer. All pumping and observation wells of the pumping test are screened in the Brussels Sands. The Brussels Sands formation is an early Middle-Eocene shallow marine sand deposit in Central Belgium (Fig. 1). Its geological features are extensively covered in Houthuys (1990) and Houthuys (2011). This aquifer is a major source of groundwater in Belgium and was studied at the regional scale by Peeters et al. (2010). The most interesting feature of these sands in terms of groundwater flow and transport is the complex geological heterogeneity originating in its depositional history. The Brussels Sands are a tidal sandbar deposit. Its deposition started when a strong SSW-NNE tidal current in the early Middle-Eocene produced longitudinal troughs, that were afterwards filled by sandbar deposits. In these sandbar deposits, sedimentary features such as cross-bedding, mud drapes and reactivation surfaces are abundantly present (Houthuys 1990; Houthuys 2011). The orientation of most of these structures is related to the NNE-orientation of the main tidal flow during deposition.

2.2 Pumping test

In February 1993, a pumping test was performed in Bierbeek (Belgium) under the authority of the company TUC RAIL N.V. in the framework of high-speed train infrastructure works. One pumping well (PP1) and six observations wells were drilled in the 35m-thick coarse facies of the Brussels Sands (Figure 3). The observation wells are situated between 4m and 75m from the pumping well and are located in different orientations. Before pumping the water table was at 49.8 m. During the pumping test, there was 72 hours of pumping in well PP1 with a flow rate of 2120 m^3/day. Water level in six observation wells was continuously monitored during pumping and during an additional 24 hours of recovery after pumping. The pumping test was interpreted by inverse modelling using a numerical method described in Lebbe and De Breuck (1995). This analysis showed that the best calibration was obtained assuming horizontal anisotropy in the coarse facies of the Brussels Sands. The maximal horizontal hydraulic conductivity was found to be 28.3 m/day while the minimal horizontal hydraulic conductivity was 13.4 m/day. The principal direction of maximal horizontal hydraulic conductivity corresponds to N 115°48’ E (TUC RAIL N.V., 1993). This principal orientation is exactly perpendicular to the SSW-NNE orientation of the main tidal flow during deposition and the mud drapes in the Brussels Sands.

2.3 In situ mapping and measurement of clay drape properties

The Brussels Sands outcrops in the Bierbeek quarry are used as an analog for the Brussels Sands found in the subsurface at the pumping test site. This quarry is located at approximately 500 m from the pumping test site (Figure 1). This outcrop of approximately 1200 m² was mapped in detail with regard to the spatial distribution of sedimentary structures and permeability in Huysmans et al. (2008). A total of 2750 cm-scale air permeability measurements were carried out in situ on different faces of the Bierbeek quarry to characterize the spatial distribution of permeability. From the hydrogeological point of view in the present study, the main interest lies in the occurrence and geometry of structures with high and low hydraulic conductivity. In this perspective, the Brussels Sands can be regarded as consisting of horizontal permeable sand layers of approximately 1m thick intercalated by horizontal low-permeable clay-rich bottomsets and inclined low-permeable clay drapes. Figure 4 shows a field picture and a geological interpretation of the typical clay-sand patterns in the Bierbeek quarry. More details about the spatial distribution of the fine-scale sedimentary structures and measured permeability in the Brussels Sands can be found in Huysmans et al. (2008).

2.4 Training image construction

The observed spatial patterns of clay drape occurrence are explicitly represented in a training image. Training images are essential to multiple-point geostatistics. In multiple-point geostatistics, "training images" are used to characterize the patterns of geological heterogeneity. A training image is an explicit grid-based representation of the expected geological patterns. In the simulation step, patterns are borrowed from the training image and reproduced in the simulation domain. (Guardiano and Srivastava 1993; Strebelle and Journel, 2001; Caers and Zhang 2004). More information about the theory behind multiple-point geostatistics can be found in Strebelle (2000) and Strebelle (2002). Description of the different multiple-point algorithms can be found in the following papers: SNESIM (Strebelle 2002; Liu 2006), FILTERSIM (Zhang et al. 2006; Wu et al. 2008), SIMPAT (Arpat and Caers 2007), HOSIM (Mustapha and Dimitrakopoulos 2010) and the Direct Sampling method (Mariethoz et al. 2010).

In this study, a two-dimensional fine-scale training image of clay and sand occurrence of the Brussels Sands was constructed based on the in situ mapping in the Bierbeek quarry. In the third dimension perpendicular to the 2D training image, layering and clay drapes are very continuous as shown on figure 5 which shows quarry wall pictures in the NNE-direction and the perpendicular orientation. While the picture of the NNE-oriented face displays cross-bedding and inclined mud drapes, the picture of the perpendicular face shows continuous horizontal layering (Figure 5). Therefore all layers and sedimentary structures are assumed to be continuous in that direction. The incorporation of 3D simulations based on several 2D training images in different directions following the approaches discussed in Comunian et al. (2012) could be interesting future work. The two-dimensional fine-scale training image along the NNE-direction (Figure 6) shows an alternation of sand-rich and clay-rich zones. More details about construction of this training image can be found in Huysmans and Dassargues (2009). This training image will be used in section 2.6 where multiple-point statistics are borrowed from this training image to simulate realizations of clay drape occurrence to be used as input for the local groundwater flow model.

2.5 Groundwater flow model

The groundwater flow model is a three-dimensional local model of 600m x 600 m x 30.4m including all pumping and observation wells from the pumping test in Bierbeek described in section 2.2. The size of the model in the horizontal direction was chosen to be 600 m since analysis of the pumping test data showed that no drawdown is measured at 300 m from the pumping well (TUCRAIL N.V., 1993). The model is oriented along the N22.5°E direction which is parallel to the direction of the main geological structures and the main anisotropy axis of the observed drawdowns from the pumping test. The top of the Ieper Clay deposits represents the impermeable bottom of the model due to the low permeability of this unit (Huysmans and Dassargues, 2006). The top of the model corresponds to an elevation of 49.8 m, which corresponds to the initial groundwater level before pumping. This means that only one geological layer is present in the model, i.e., the Brussels Sands. The model consists of a central inner zone of 55m x 100m x 15.3m including all well screens and an outer zone (Figure 7). This inner zone consists of 51 cells in the x-direction, 183 cells in the y-direction and 51 layers. In the central inner zone where all the well screens are situated, a very small grid cell size of 0.3m x 0.3m x 0.3m is adopted so that individual clay drapes can be explicitly incorporated in the model in this zone. In the outer zone, larger grid cell sizes between 0.45m and 82m in the horizontal direction and layer thicknesses between 3m and 6m are chosen. For numerical reasons, the dimensions of the grid cells do not exceed 1.5 times the dimensions of their neighboring cells. The total model consists of 213 cells in the x-direction, 361 cells in the y-direction and 54 layers. The total number of grid cells in the model is thus 4,152,222 cells. The model is run in transient conditions with a total time length of 4510 minutes subdivided into 99 time intervals. Piezometric heads are prescribed at the lateral boundaries of all model layers. In the pumping well PP1, a pumping rate of 2120 m^3/day is applied during

72 hours. Initial hydraulic conductivity and storage parameters were taken from a previous interpretation (TUCRAIL N.V., 1993) and calibrated afterwards. A total of 594 observed heads measured in six observation wells (Figure 3) from two minutes after the start of pumping until 240 minutes after stopping of pumping are available for calibration. The differential equations describing groundwater flow are solved by PMWIN (Chiang and Kinzelbach 2001), which is a pre- and post-processor for MODFLOW (McDonald and Harbaugh 1988), using a block-centered, finite-difference, method.

Two model variants are run and calibrated separately. First, a homogeneous and horizontally isotropic model without clay drapes is run. In this model, different values for horizontal and vertical hydraulic conductivity are allowed, but no anisotropy of hydraulic conductivity in the horizontal direction is introduced. Calibration is performed for adapting values of horizontal hydraulic conductivity, vertical hydraulic conductivity and specific storage. The second model incorporates a random clay drape realization as described in section 2.6. In this model, calibration of the following additional parameters is performed: clay drape thickness and clay drape hydraulic conductivity in model layers 4 to 54 and anisotropy factor of shallow layers 1 to 3 in which clay drapes are not explicitly incorporated. In layers 1 to 3 clay drapes are not explicitly incorporated since these belong to the outer zone of the model The spatial distribution of the clay drapes is not changed during calibration. Storage is assumed identical in the sand and the clay drapes. In this model, the only heterogeneity and anisotropy of hydraulic conductivity is related to the presence of clay drapes. Background hydraulic conductivity of layers 4 to 54 is homogeneous and isotropic so that the effect of clay drapes on hydraulic heads can be determined without influence of other heterogeneity or anisotropy effects. By comparing the results of these two model variants, the effects of clay drapes on the piezometric depression cone and on the calibration results can be quantified. This approach of comparing a heterogeneous model with a homogeneous equivalent was for example also applied in Mariethoz et al. (2009). For both models, a two-step calibration procedure is adopted. First, a sensitivity analysis and trial-and-error subjective calibration is performed and second, the optimal model from manual calibration is further calibrated using PEST (Doherty et al. 1994). The sensitivity analysis consists of varying the adjustable parameters (horizontal hydraulic conductivity, vertical hydraulic conductivity, specific storage and clay drape parameters) and assessing their effect on simulated drawdowns.

2.6 Clay drapes simulation using multiple-point geostatistical simulation of edge properties

In order to incorporate clay drapes showing patterns similar to the training image of Figure 6 (left) in the groundwater flow model, the technique of direct multiple-point geostatistical simulation of edge properties (Huysmans and Dassargues 2011) is used. This technique was designed to simulate thin complex surfaces such as clay drapes with a smaller CPU and RAM demand than the conventional multiple-point statistical methods. Instead of pixel values, edge properties indicating the presence of irregularly-shaped surfaces are simulated using multiple-point geostatistical simulation algorithms. The training image is upscaled by representing clay drapes as edge properties between cells instead of representing them as objects consisting of several cells. The concept of the edge of a flow model and the associated edge properties was introduced in the work of Stright (2006) as an additional variable. The edge properties are assigned to the cell faces. The cell property used in this study is the presence of clay drapes along cell faces. More details about the method can be found in Huysmans and Dassargues (2011). Figure 6 shows how the fine-scale pixel-based training image (left) is converted into an upscaled edge-based training image (right). The fine-scale training image has a grid cell size of 0.05 m and represents the clay drapes as consisting of pixels with a different pixel value than the background material. The upscaled edge-based training image has a grid cell size of 0.30 m and represents the clay drapes as edge properties that indicate the presence of clay drapes along the edges of all grid cells.

In this study, the upscaled 30 m by 30 m training image from Figure 6 (right) is used as input to SNESIM from SGeMS (Remy et al. 2009) to simulate clay drape realizations to be imported in the inner central zone of the model where individual clay drapes are incorporated. Vertical 2D realizations of 54.9m by 15.3m are generated. Figure 7 shows a random clay drape realization that is incorporated in the groundwater flow model.

The realizations of clay drape presence can be imported in the groundwater flow code PMWIN using the Horizontal-Flow Barrier (HBF) package and the vertical leakance array (VCONT array). The HBF package simulates thin vertical low-permeability geological features, which impede horizontal groundwater flow. They are situated on the boundaries between pairs of adjacent cells in the finite-difference grid (Hsieh and Freckleton, 1993). A horizontal-flow barrier is defined by assigning the barrier direction, which indicates the cell face where the barrier is located, and barrier hydraulic conductivity divided by the thickness of the barrier (Chiang and Kinzelbach, 2001). Horizontal edges are inserted into PMWIN by adapting vertical leakance (VCONT array) between two model layers. The VCONT matrix for every model layer is calculated as

$$VCONT = \frac{2}{\frac{\Delta z_u}{(K_z)_u} + \frac{\Delta z_c}{(K_z)_c} + \frac{\Delta z_l}{(K_z)_l}} \quad (1)$$

where K is hydraulic conductivity, Δz is thickness and u, c and l respectively represent the upper layer, semi-confining unit and lower layer as indicated on figure 8. In case a horizontal edge is present in a model cell, the edge is inserted in the model as a semi-confining unit. Initially, it is assumed that all clay drapes in the groundwater flow model have a thickness of 0.02 m and a hydraulic conductivity of 0.283 m/d. As mentioned previously, these values are optimized during calibration.

3. Results

Figures 9 and 10 show the resulting model outputs from the homogeneous model and the clay drape model. For both models, automatic calibration using PEST did not result in lower calibration errors, possibly as a result of the large size (4,152,222 grid cells) and complexity of the models. Manual calibration was apparently able to identify a good local minimum, possibly due to the small number of calibrated variables. In the homogeneous and horizontally isotropic model, the best calibration results were obtained with the following set of calibrated parameter values: horizontal hydraulic conductivity of 22.2 m/day, vertical hydraulic conductivity of 4.8 m/day and specific storage of 3×10^{-5} m^{-1}. In the clay drape model, the best calibration results were obtained with the following set of calibrated parameter values: horizontal hydraulic conductivity of 23 m/day vertical hydraulic conductivity of 4 m/day, specific storage of 3×10^{-5} $m^{-1}$and a clay drape parameter (hydraulic conductivity of drapes divided by drape thickness) with values between 0.175 and 9.905 day^{-1}. This clay drape parameter varied between the different sublayers of the inner zone of the model reflecting the alteration between layers with thicker or less permeable clay drapes and layers with thinner or more permeable clay drapes. In every layer, a single clay drape parameter was assigned, thus not allowing spatial variation of the clay drape parameter within the model layers.

Figure 9 shows piezometric maps at z = 27 m amsl, i.e., located at the depth of the centre of the pumping well screen, for (1) the homogeneous and horizontally isotropic model and (2) the clay drape model. Figure 9A shows circular hydraulic head contours indicating an isotropic piezometric pumping depression cone resulting from the homogeneity and isotropy of hydraulic conductivity in the horizontal direction. Figure 9B shows the hydraulic head contours for the second model which incorporates clay drapes. These contours are elliptical demonstrating an anisotropic pumping depression cone. The vertical clay drapes cause bending of the hydraulic head contours. Since no other K heterogeneity than the clay drape presence is incorporated in the model, these results show that anisotropic pumping cones at large-scale can be attributed to the presence of fine-scale clay drapes.

Figure 10 shows calculated versus observed drawdown graphs for (1) the homogeneous and horizontally isotropic model variant and (2) the clay drape model variant. Figure 11 shows calculated and observed drawdown versus time for (1) the homogeneous and horizontally isotropic model variant and (2) the clay drape model variant The error variance for the isotropic model is 1.24 E-2 m², while the error variance for the clay drape model is as low as 7.292E-3 m². The residual mean of the homogeneous and isotropic model is -3.08 E-2 m, while the residual mean for the clay drape model is -2.12 E-2 m. Correlation coefficient between observed and simulated drawdowns increases from 0.9906 (homogeneous/isotropic model) to 0.9916 (clay drape model). Incorporating the clay drapes thus results in a better fitting between calculated and observed drawdown values for this pumping test. Especially the larger drawdowns are better reproduced in the clay drape model. This is most obvious on figure 11 which shows that time behaviour is generally well reproduced by the model but that larger drawdowns are better reproduced in the clay drape model. These large drawdowns are measured in observation well PB1.2 which is located close to the pumping well (Figure 3). In the clay drape model, a clay drape is present in the pumped layer between the pumping well and observation well PB1.2 which acts as a flow barrier between those two wells. The presence of this barrier results in a better reproduction of the measured drawdowns by the model.

4. Discussion and conclusion

This study has investigated the effect of fine-scale clay drapes on pumping test response. For this purpose, spatial distribution and geometry of clay drapes observed in a cross-bedded aquifer were explicitly incorporated in a local groundwater model of a pumping test site. Clay drape parameters were calibrated in order to reproduce hydraulic head measurements observed during a pumping test. Best calibration results were obtained with a zoned clay drape parameter or drape leakage coefficient, defined as hydraulic conductivity of drapes divided by drape thickness, with values between 0.175 and 9.905 day^{-1}. If the clay drape thickness is assumed to be 0.02 m, this means that hydraulic conductivity of the clay drapes is between 0.0035 m/day (= 4.05×10^{-8} m/s) and 0.1981 m/day (= 2.29×10^{-6} m/s). These values lie in the hydraulic conductivity interval of silt and silty sand respectively according to Fetter (2001), so these values are realistic and are certainly not chosen unrealistically low. This implies that the anisotropic pumping cone can be reproduced and explained with realistic values for clay drape thickness and hydraulic conductivity andthat fine-scale clay drapes can cause an anisotropic pumping test response at a much larger scale.

Incorporating clay drapes in groundwater models is challenging since they are often irregular curvilinear three-dimensional surfaces which may display a very complex spatial distribution. In this paper, a combined approach of multiple-point geostatistics and edge properties was used to incorporate the clay drapes in the flow model. Clay drapes were represented as grid cell edge properties instead of representing them by pixels. This allowed modelling with a larger grid cell size and thus a smaller CPU and RAM demand. A realistic spatial distribution of clay drape occurence was simulated using multiple-point geostatistics based on a field-based training image. This combined approach of multiple-point geostatistics and edge properties has shown to be an efficient and valid approach since realistic spatial patterns and geometry of the clay drapes can be preserved in the model without having to represent each clay drape by pixels.

In order to determine the added value of explicitly incorporating clay drape presence in the flow model for pumping test interpretation, the model was also compared with a homogeneous and isotropic model calibrated on the same pumping test data. Incorporating the clay drapes resulted in a better fit between calculated and observed drawdown values than the homogeneous model.

Acknowledgements

The authors wish to acknowledge the Fund for Scientific Research – Flanders for providing a Postdoctoral Fellowship to the first author. We thank TUCRAIL for providing the pumping test data.

References

Arpat, G.B. and J. Caers (2007) Conditional simulation with patterns, Mathematical Geology 39(2): 177-203.

Bayer, P., Huggenberger, P., Renard, P. and A. Comunian (2011) Three-dimensional high resolution fluvio-glacial aquifer analog: Part 1: Field study, J. Hydrol. 405(1-2), 1-9.

Beliveau, D. (2002), Reservoir heterogeneity, geostatistics, horizontal wells, and black jack poker, AAPG Bulletin 86 (10), 1847– 1848.

Caers, J., and T. Zhang (2004), Multiple-point geostatistics: a quantitative vehicle for integrating geologic analogs into multiple reservoir models, In: Integration of outcrop and modern analog data in reservoir models, AAPG memoir, vol 80, pp 383–394.

Chiang, W., and W. Kinzelbach (2001), 3D-groundwater modeling with PMWIN, Springer, Berlin. ISBN 3-540-67744-5.

Comunian, A., Renard, P., Straubhaar, J. and Bayer P. (2011) Three-dimensional high resolution fluvio-glacial aquifer analog – Part 2: Geostatistical modeling, Journal of Hydrology 405(1-2): 10-23.

Comunian, A., Renard, P., Straubhaar, J. (2012) 3D multiple-point statistics simulation using 2D training images. Computers and Geosciences 40, 49-65.

dell'Arciprete, D., Bersezio, R., Felletti, F., Giudici, M., Comunian, A., Renard, P. (2012), Comparison of three geostatistical methods for hydrofacies simulation: a test on alluvial sediments, Hydrogeol J 20, 299-311.

Doherty, J., Brebber, L., and P. Whyte (1994), PEST - Model-independent parameter estimation. User's manual. Watermark Computing. Australia.

Eaton, T.T. (2006), On the importance of geological heterogeneity for flow simulation, Sed Geol 184, 187–201.

Farmer, C.L. (2002), Upscaling: a review, Int J Num Meth Fluids 40(1-2), 63-78.

Feyen, L. And J. Caers (2006), Quantifying geological uncertainty for f low and transport modeling in multi-modal heterogeneous formations, Adv Water Resour 29(6), 912-929.

Fetter, C.W. (2001), Applied hydrogeology, Prentice-Hall, New Yersey, 598 p.

Fogg, G.E., Noyes, C.D. and S.F. Carle (1998), Geologically based model of heterogeneous hydraulic conductivity in an alluvial setting, Hydrogeol J 6(1), 131–143.

Guardiano, F. And M. Srivastava(1993), Multivariate geostatistics: beyond bivariate moments, In: Soares A (ed) Geostatistics-Troia. Kluwer Academic, Dordrecht.

Harp, D.R. and V.V. Vesselinov (2011), Identification of Pumping Influences in Long-Term Water Level Fluctuations, Ground Water 49(3), 403-414.

Hendricks Franssen, H.-J. and F. Stauffer (2005), Inverse stochastic estimation of well capture zones with application to the Lauswiesen site (Tübingen, Germany), In Renard P., Demougeot-Renard H. and Froidevaux R. (Eds), Geostatistics for Environmental Applications, Proceedings of the Fifth European Conference on Geostatistics for Environmental Applications, Springer-Verlag, Berlin, Heidelberg.

Herweijer, J. (1996), Constraining uncertainty of groundwater flow and transport models using pumping tests, in Calibration and Reliability in Groundwater Modelling, pp. 473{482, IAHS Publ., 237.

Houthuys, R. (1990), Vergelijkende studie van de afzettingsstruktuur van getijdenzanden uit het Eoceen en van de huidige Vlaamse banken, Aardkundige Mededelingen 5, Leuven University Press, p. 137.

Houthuys, R. (2011), A sedimentary model of the Brussels Sands, Eocene, Belgium, Geologica Belgica 14(1-2), 55-74.

Hsieh, P.A., and J.R. Freckleton (1993), Documentation of a computer program to simulate horizontal-flow barriers using the U.S. Geological Survey's modular three-dimensional finite-difference ground water flow model, U.S. Geological Survey Open File Report 92-477.

Hu, L.Y., and T. Chugunova (2008), Multiple-point geostatistics for modeling subsurface heterogeneity: a comprehensive review, Water Resour Res 44:W11413, doi:10.1029/2008WR006993.

Huysmans, M., and A. Dassargues (2006), Hydrogeological modeling of radionuclide transport in low permeability media: a comparison between Boom Clay and Ypresian Clay, Env Geol, 50 (1), 122-131

Huysmans, M., and A. Dassargues (2009), Application of multiple-point geostatistics on modeling groundwater flow and transport in a cross-bedded aquifer, Hydrogeol J 17(8), 1901-1911

Huysmans, M., and A. Dassargues (2011), Direct multiple-point geostatistical simulation of edge properties for modelling thin irregularly-shaped surfaces, Math Geosci 43 (5), 521-536

Huysmans, M., Peeters, L., Moermans, G., and A. Dassargues (2008), Relating small-scale sedimentary structures and permeability in a cross-bedded aquifer, J Hydrol 361, 41-51

Journel, A. and T. Zhang (2006), The necessity of a multiple-point prior model, Math Geol 38(5), 591–610.

Kollet, S.J. and V.A. Zlotnik (2005), Influence of aquifer heterogeneity and return flow on pumping test data interpretation, J Hydrol 300(1-4), 267-285

Koltermann, C.E. and S. Gorelick (1996), Heterogeneity in sedimentary deposits: a review of structure imitating, process-imitation, and descriptive approaches, Water Resour Res 32(9), 2617–2658.

Lavenue, M. and G. de Marsily (2001), Three-dimensional interference test interpretation in a fractured aquifer using the pilot point inverse method, Water Resour Res 37(11), 2659-2675

Lebbe, L. and W. Debreuck (1995), Validation of an inverse numerical model for interpretation of pumping tests and a study of factors influencing accuracy of results, J Hydrol 172(1-4), 61-85

Le Coz, M., Genthon, P., and P.M. Adler (2011), Multiple-point statistics for modeling facies heterogeneities in a porous medium: the Komadugu-Yobe Alluvium, Lake Chad Basin, Math. Geosci. 43, 861-878.

Li, H.M. and J. Caers (2011), Geological modelling and history matching of multi-scale flow barriers in channelized reservoirs: methodology and application, Petroleum Geoscience 17(1): 17-34.

Liu, Y. (2006), Using the Snesim program for multiple-point statistical simulation, Comput Geosci 32(10):1544–1563

Mariethoz, G., Renard, P., Cornaton, F., Jacquet, O. (2009), Truncated plurigaussian simulations to characterize aquifer heterogeneity, Ground Water 47(1), 13-24.

Mariethoz, G., Renard, P. and J. Straubhaar (2010), The Direct Sampling method to perform multiple-point geostatistical simulations, Water Resour Res, 46, W11536, DOI: 10.1029/2008WR007621

McDonald, M.G., and A.W. Harbaugh (1988), A modular three-dimensional finite-difference ground-water flow model, Technical report USGS, Reston, VA

Mikes, D. (2006), Sampling procedure for small-scale heterogeneities (crossbedding) for reservoir modeling, Mar. Petrol. Geol. 23 (9-10), 961-977.

Morton, K., Thomas, S., Corbett, P., and D. Davies (2002), Detailed analysis of probe permeameter and vertical inteference test permeability measurements in a heterogeneous reservoir, Petrol. Geosci. 8, 209-216.

Mustapha, H. and R. Dimitrakopoulos (2010), High-order stochastic simulation of complex spatially distributed natural phenomena, Math Geosci 42:457–485.

Neuman, S.P. (2003), Multifaceted nature of hydrogeologic scaling and its interpretation, Reviews of Geophysics 41 (3), 4.1– 4.31.

Peeters, L., Fasbender, D., Batelaan, O. and A. Dassargues (2010), Bayesian Data Fusion for water table interpolation: incorporating a hydrogeological conceptual model in kriging, Water Resour Res 46(8), DOI:10.1029/2009WR008353

Reineck, H.-E. and I. B. Singh (1973), Depositional sedimentary environments, Springer-Verlag, Berlin, New York, 439 p.

Remy, N., Boucher, A. And J. Wu (2009) Applied Geostatistics with SGeMS – a user's guide, Cambridge University Press, New York, 264 p.

Renard, Ph. and G. de Marsily (1997), Calculating equivalent permeability: a review, Adv Water Resour 20 (5-6): 253-278

Ringrose, P.S., Sorbie, K.S., Corbett, P. W. M. and J.L. Jensen (1993) Immiscible flow behaviour in laminated and cross-bedded sandstones, Journal of Petroleum Science and Engineering 9 (2): 103-124.

Ronayne, M.J., Gorelick, S.M., and J. Caers (2008,) Identifying discrete geologic structures that produce anomalous hydraulic response: An inverse modeling approach, Water Resour Res 44(8), DOI: 10.1029/2007WR006635

Schulze-Makuch, D. and D.S. Cherkauer (1998) Variations in hydraulic conductivity with scale of measurement during aquifer tests in heterogeneous, porous carbonate rocks, Hydrogeol J 6 (2), 204– 215.

Schulze-Makuch, D., Carlson, D.A., Cherkauer, D.S., and P. Malik (1999), Scale depency of hydraulic conductivity in heterogeneous media, Ground Water 37(6), 904-919

J. Straubhaar, P. Renard, G. Mariethoz, R. Froidevaux, O. Besson (2011), An improved parallel multiple-point algorithm using a list approach, Math. Geosci. 43(3), 305–328.

Strebelle, S. (2000), Sequential simulation drawing structures from training images, Doctoral dissertation, Stanford University.

Strebelle, S. and A.G. Journel (2001) Reservoir modeling using multiple-point statistics. SPE Annual Technical conference and Exhibition, New Orleans, Sept. 30 – Oct. 3, 2001, SPE # 71324.

Strebelle, S. (2002), Conditional simulation of complex geological structures using multiple-point statistics, Math Geol 34:1–22.

Stright, L., (2006) Modeling, Upscaling and History Matching Thin, Irregularly-Shaped Flow Barriers; A Comprehensive Approach for Predicting Reservoir Connectivity, SPE Paper 106528.

TUC RAIL N.V. (1993), Studie van de invloed van de tunnel voor de HSL op het groundwater van Bierbeek, internal report.

Van den Berg, E.H. (2003), The impact of primary sedimentary structures on groundwater flow—a multi-scale sedimentological and hydrogeological study in unconsolidated eolian dune deposits, PhD Thesis, Vrije Universiteit Amsterdam, 196 pp..

Willis, B.J. and C.D. White (2000), Quantitative outcrop data for flow simulation, J. Sediment. Res. 70, 788-802.

Wu, J., Boucher, A., and T. Zhang (2008), SGeMS code for pattern simulation of continuous and categorical variables: FILTERSIM, Comput Geosci 34:1863–1876.

Zhang, T., Switzer, P., Journel, A.G. (2006), Filter-based classification of training image patterns for spatial simulation, Math Geol 38:63–80

Figure captions

Figure 1 Map of Belgium showing Brussels Sands outcrop and subcrop area (shaded part) (modified after Houthuys (1990) and inset showing the location of the pumping test site and the Bierbeek quarry

Figure 2 Geological EW-profile through the study area, modified after Houthuys (1990)

Figure 3 Pumping test configuration showing the pumping well (white circle) and observation wells (black circles) and the orientation and delineation of the central inner zone of the local groundwater model. Observation well PB1.1 is not screened in the Brussels Sands and is therefore not used in this study.

Figure 4 Raw (left) and interpreted (right) field picture, showing foresets, bottomsets and clay drapes in the Brussels Sands observed in the Bierbeek quarry

Figure 5 (A) Photomosaic of Bierbeek quarry wall in NNE direction showing cross-bedding and quasi-horizontal clay-rich bottomsets. Height of quarry wall is approximately 4–5 m and (B) photomosaic of N45°W oriented Bierbeek quarry wall showing continuous horizontal layers. Length of quarry wall shown on picture is approximately 22 m.

Figure 6 (A) Vertical two-dimensional training image of 30 m by 30 m in NNE direction: sand facies (white), clay-rich facies (black) modified from Huysmans and Dassargues (2009) and (B) the corresponding edge training image modified from Huysmans and Dassargues (2011)

Figure 7 Groundwater flow model grid and edge realization

Figure 8 Grid configuration used for the calculation of VCONT in the presence of a horizontal clay drape between two cells (modified after Chiang and Kinzelbach 2001)

Figure 9 Piezometric maps at z = 27 m corresponding to the central level of the pumping well screen, for (A) the homogeneous and horizontally isotropic model and (B) the clay drape model showing drawdown after two days

Figure 10 Calculated versus observed drawdown graphs for (1) the homogeneous and horizontally isotropic model variant and (2) the clay drape model variant

Figure 11 Calculated and observed drawdown versus time for (A) the homogeneous and horizontally isotropic model variant and (B) the clay drape model variant

Figure 1

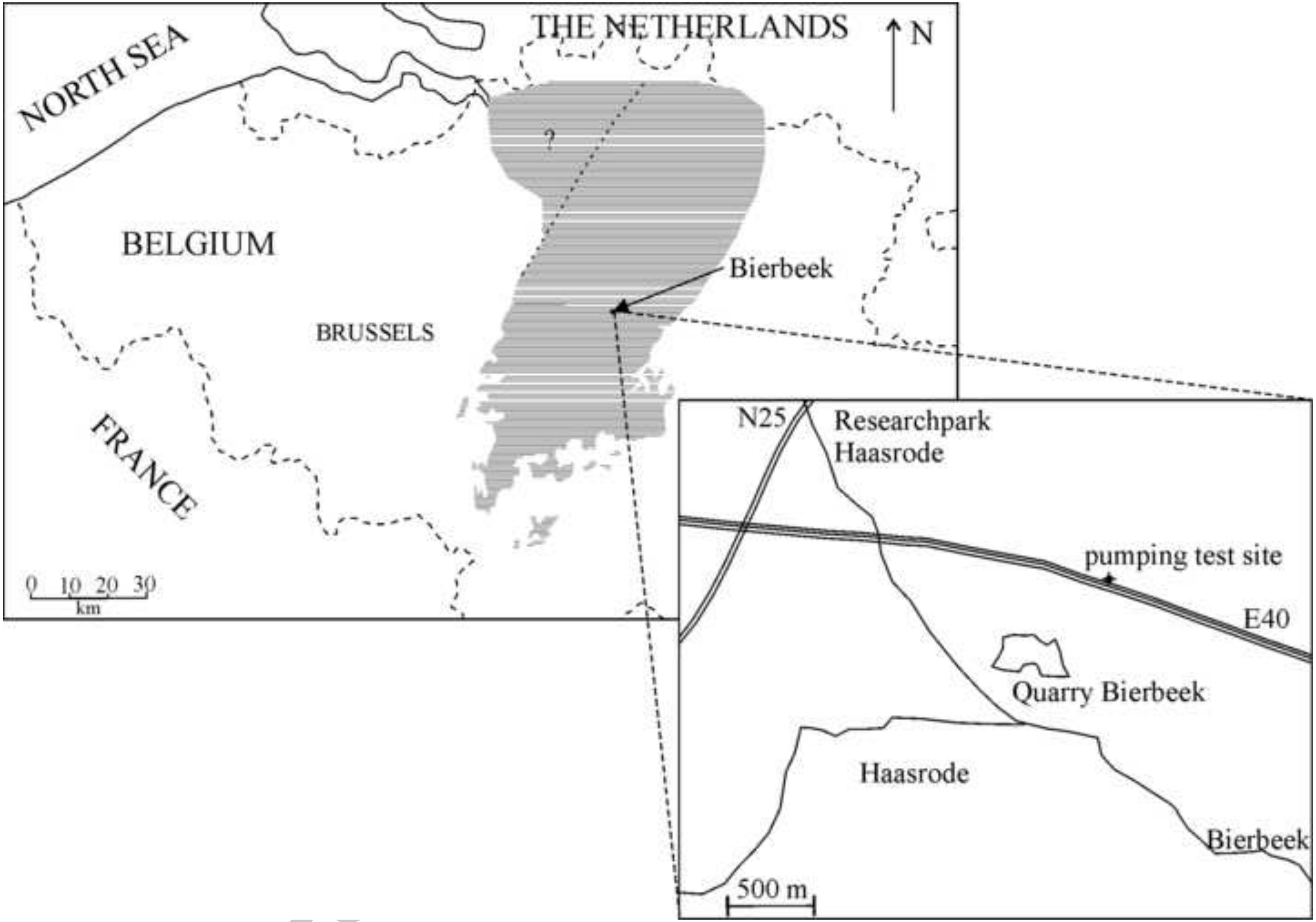
NORTH SEA
THE NETHERLANDS
N
BELGIUM
BRUSSELS
FRANCE
Bierbeek
?
0 10 20 30
km
N25
Researchpark
Haasrode
pumping test site
E40
Quarry Bierbeek
Haasrode
Bierbeek
500 m

Figure 2

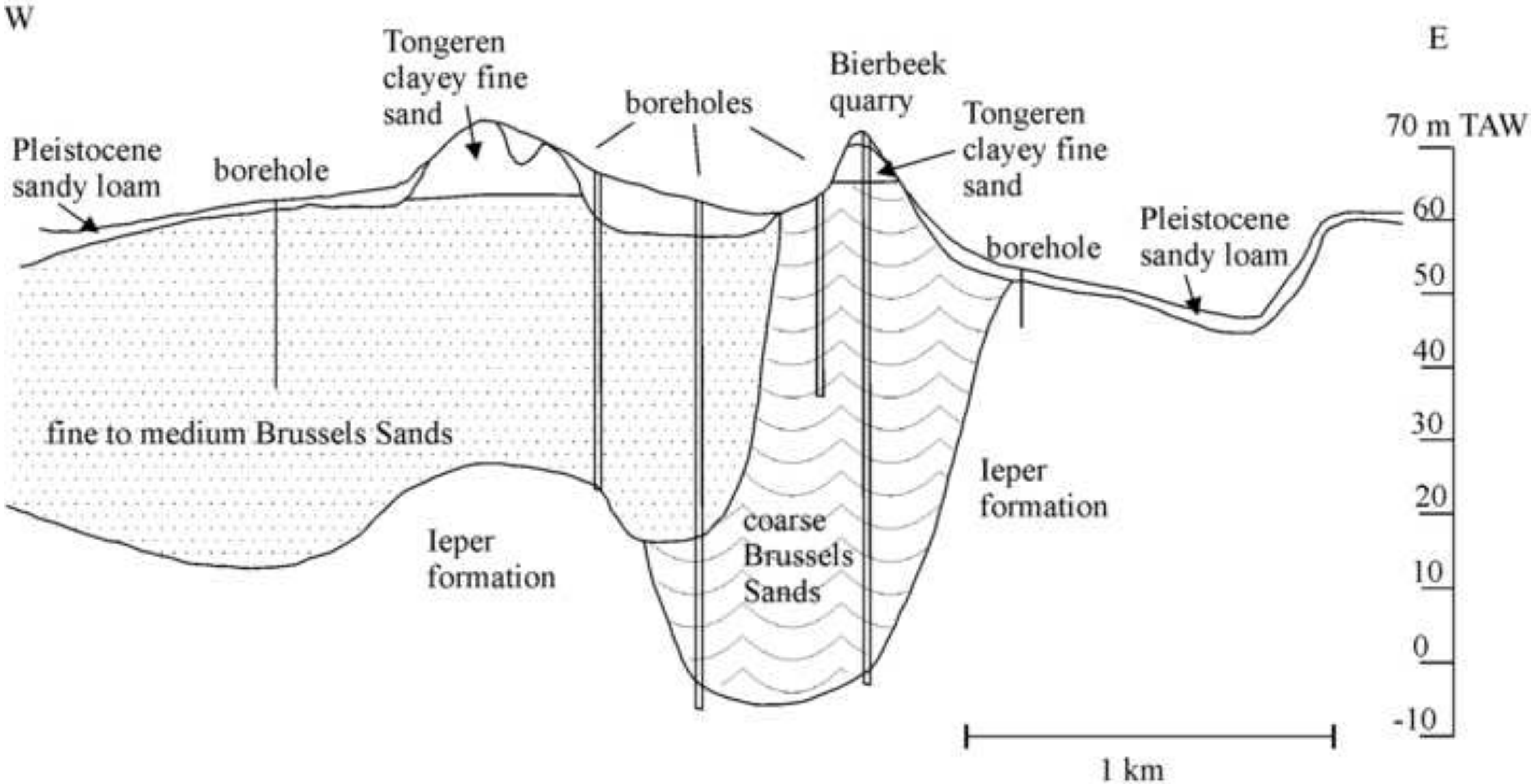
W
E
Tongeren clayey fine sand
boreholes
Bierbeek quarry
Tongeren clayey fine sand
Pleistocene sandy loam
borehole
70 m TAW
60
borehole
Pleistocene sandy loam
50
40
fine to medium Brussels Sands
30
Ieper formation
20
Ieper formation
coarse Brussels Sands
10
0
-10
1 km

Figure 3

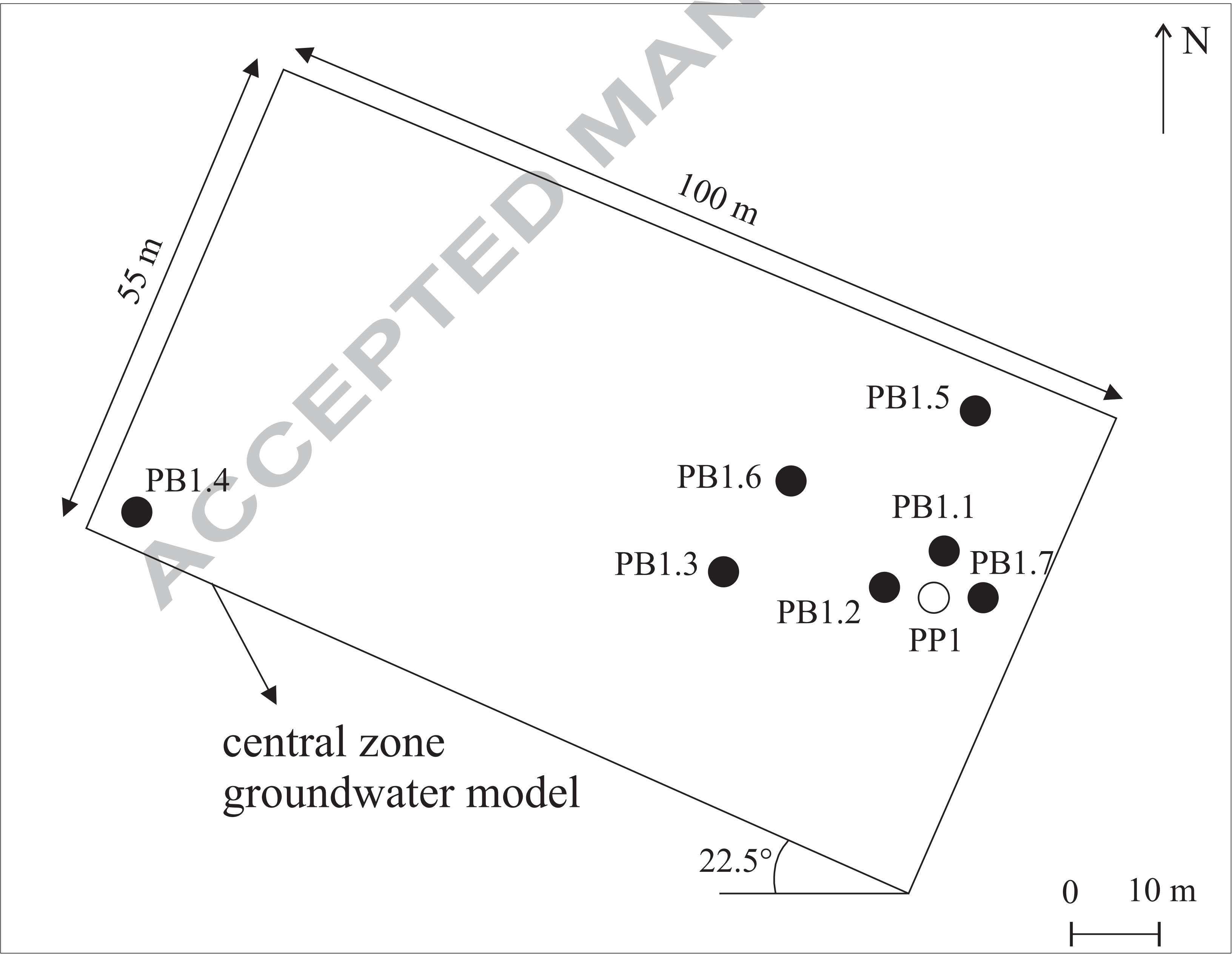
N
100 m
55 m
PB1.5
PB1.6
PB1.4
PB1.1
PB1.3
PB1.7
PB1.2
PP1
central zone
groundwater model
22.5°
0
10 m

Figure 4

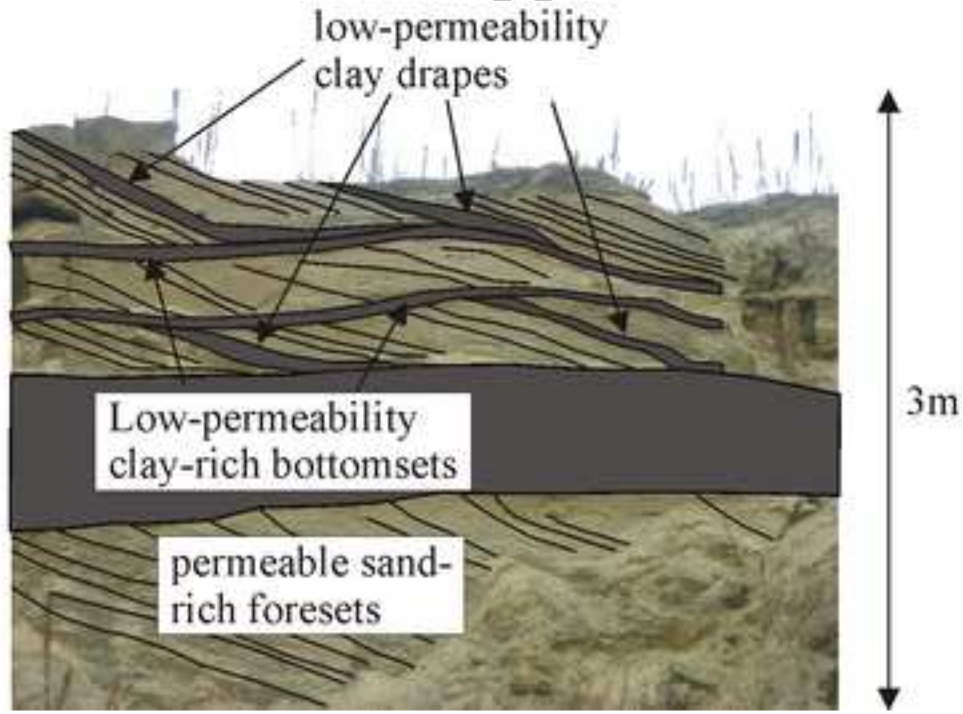
low-permeability
clay drapes
Low-permeability
clay-rich bottomsets
permeable sand-
rich foresets
3m

Figure 5

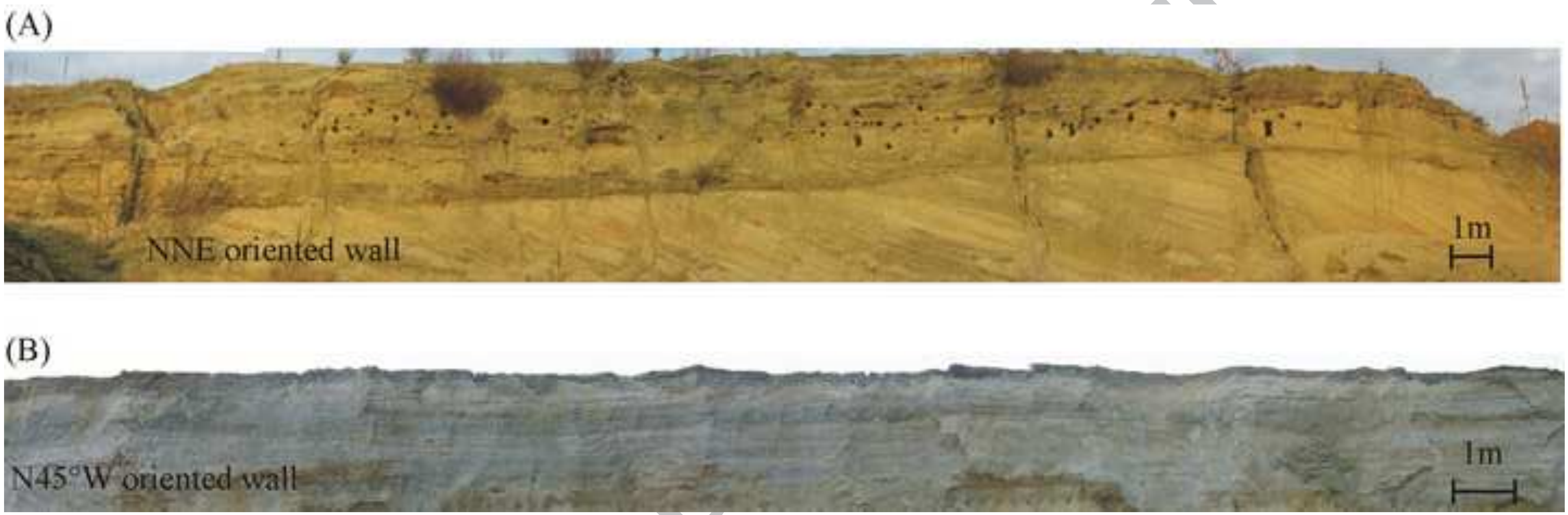

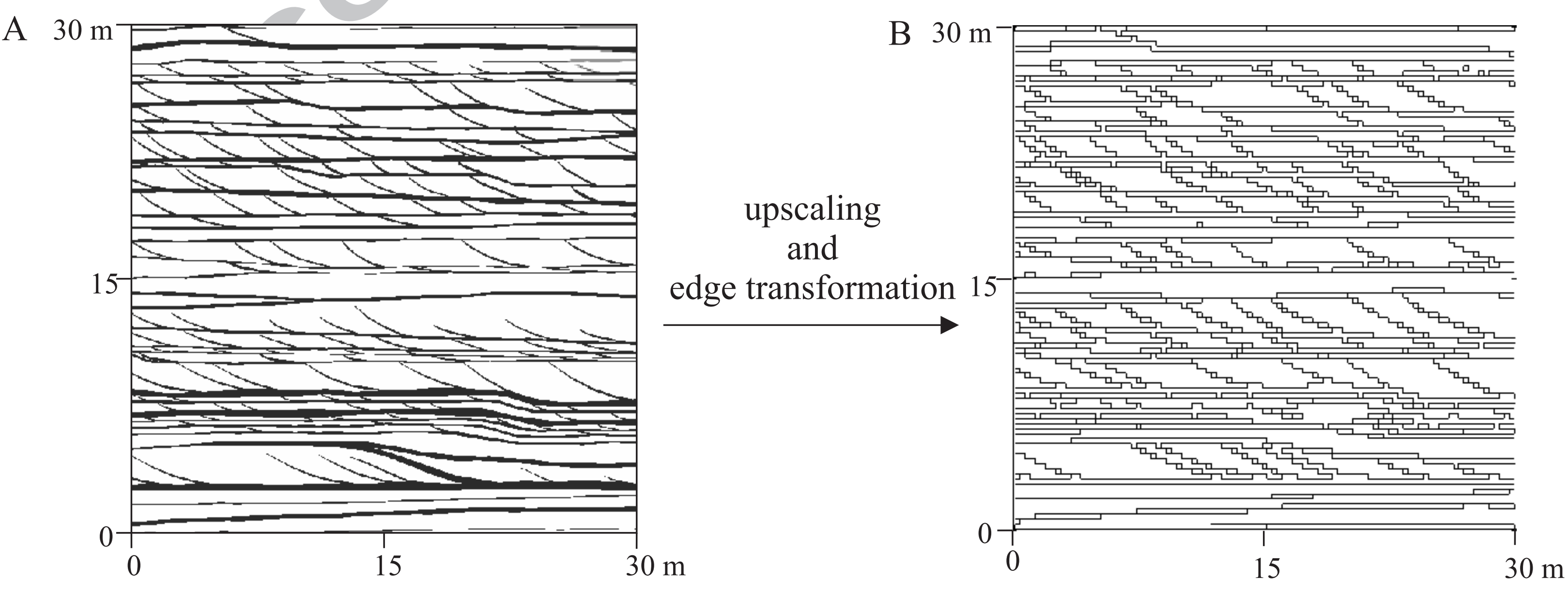
A
30 m
15
0
0
15
30 m
upscaling
and
edge transformation
B
30 m
15
0
0
15
30 m

Figure 7

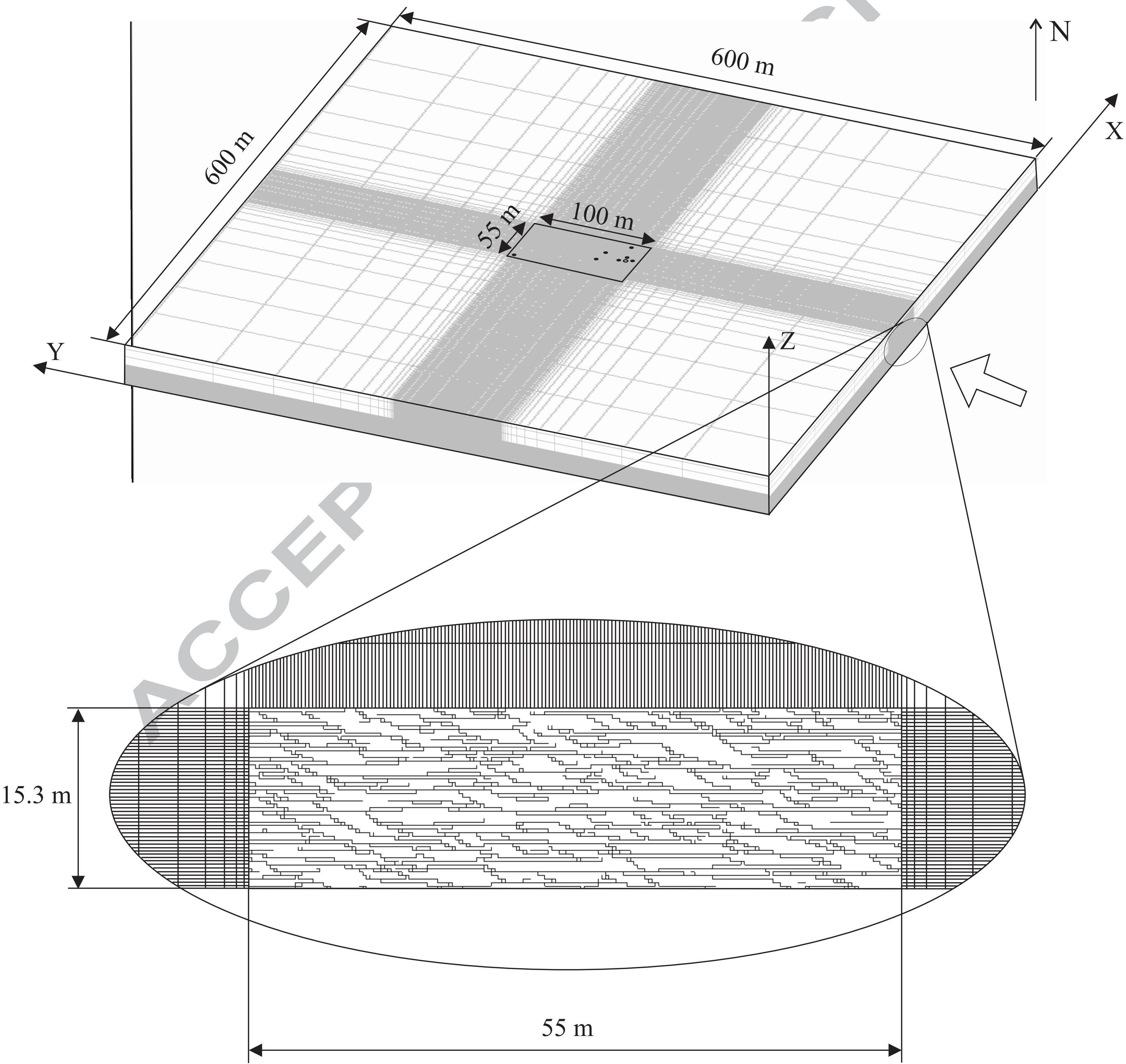

Figure 8

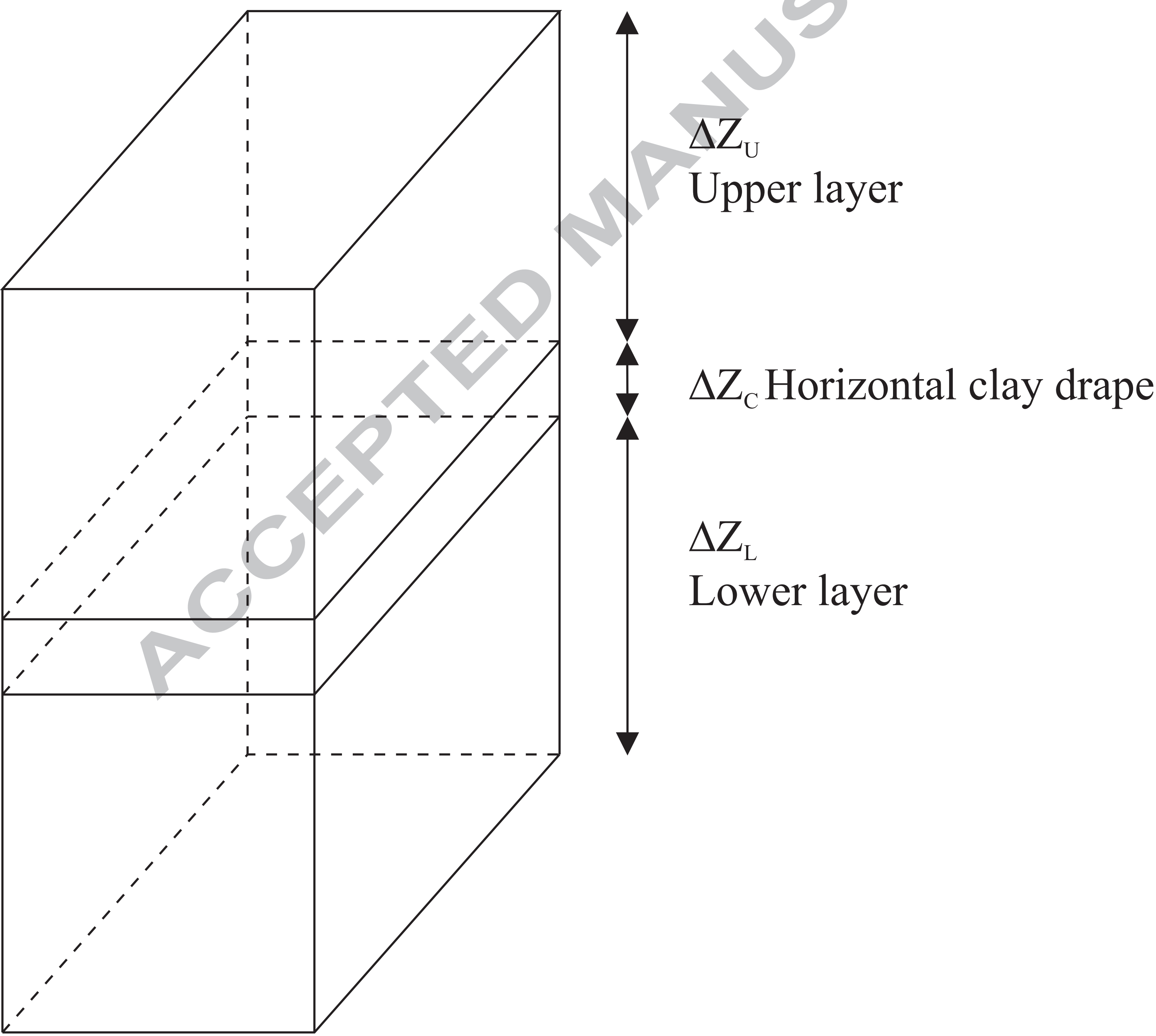

ΔZ_U
Upper layer
ΔZ_C Horizontal clay drape
ΔZ_L
Lower layer

Figure 9

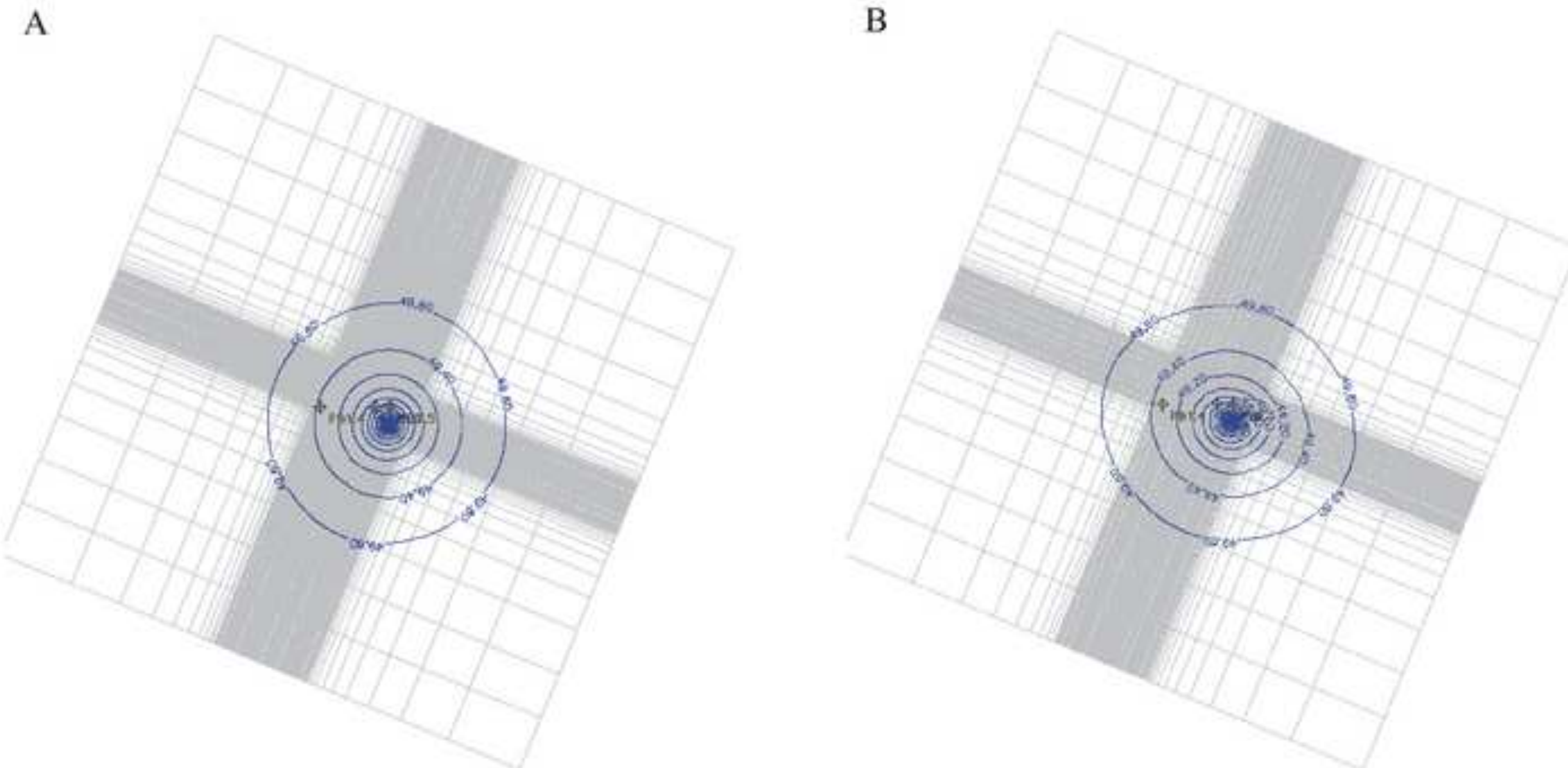

Figure 10

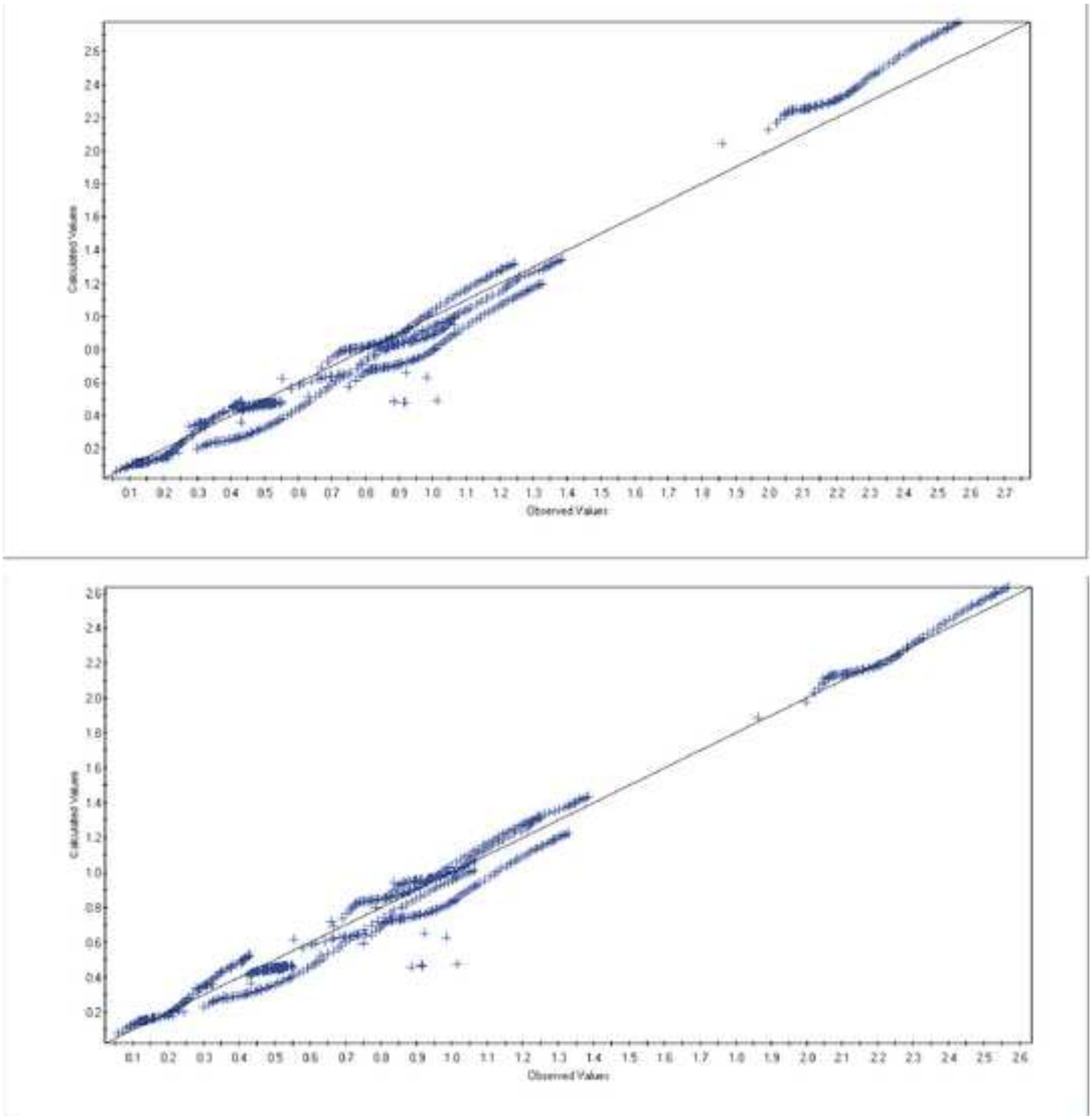
Calculated Values
Observed Values
Calculated Values
Observed Values

Figure 11

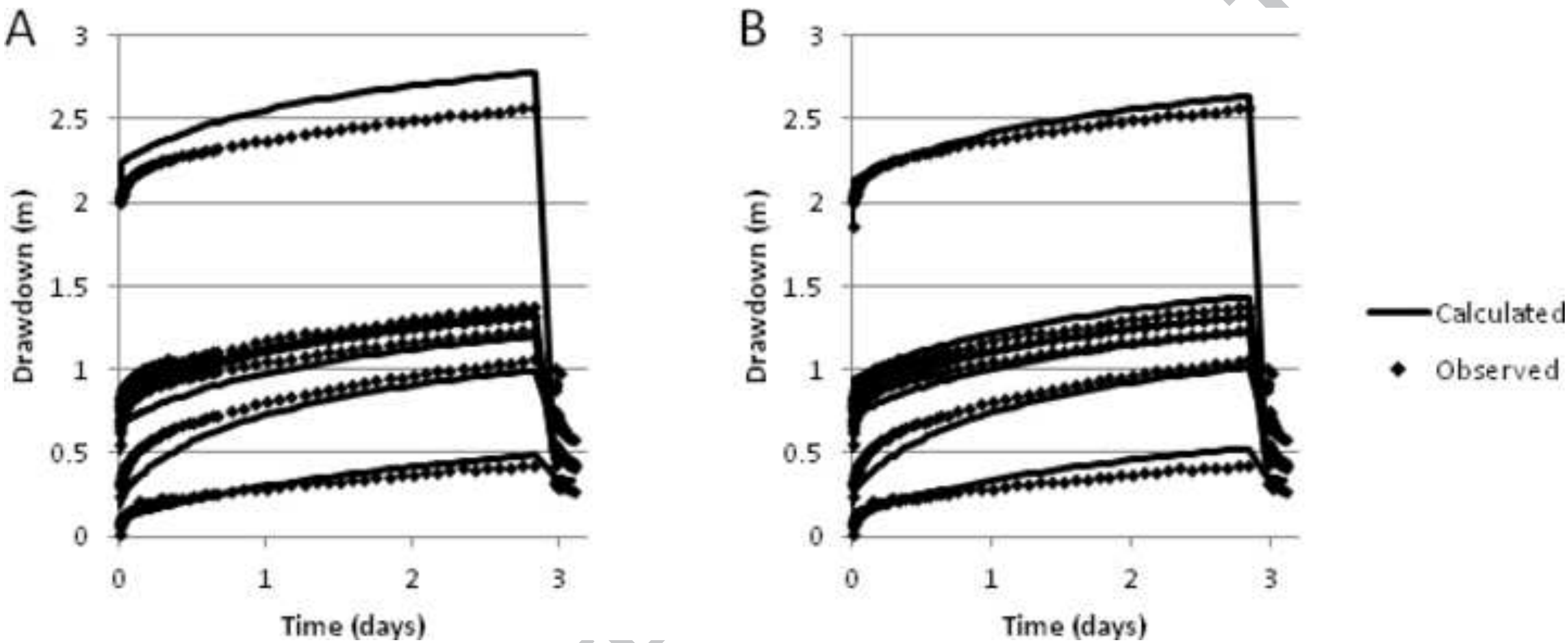

A
B
3
2.5
2
1.5
1
0.5
0
Drawdown (m)
0
1
2
3
Time (days)
Calculated
Observed

Highlight 1: Small-scale clay drapes can cause anisotropic pumping test response at larger scale

Highlight 2: An approach using multiple-point geostatistics and edge properties is proposed

Highlight 3: Incorporating small-scale clay drapes results in a better fit of drawdowns